MODELLING OF WIND TUNNEL INTERFERENCE ON HELICOPTER MEASUREMENTS AND ASSESSMENT OF THE CURRENTLY USED CORRECTIONS BASED ON THE HELINOVI DATABASE

Vasilis A. Riziotis[1] and Spyros G. Voutsinas[2]

[1] National Technical University of Athens, NTUA
Heroon Polytechniou 9, 15773 Athens Greece
e-mail: vasilis@fluid.mech.ntua.gr

[2] National Technical University of Athens, NTUA
Heroon Polytechniou 9, 15773 Athens Greece
e-mail: spyros@fluid.mech.ntua.gr

Key words: Open jet wind tunnel interference, aeroelastic modelling of helicopters, vortex methods, vibration analysis, HeliNoVi

Abstract: Wind tunnel tests on scaled helicopter models in combination with advanced numerical simulations constitute the two powerful tools of modern applied rotorcraft research. In spite of the substantial progress made on both over the last years, there are still some open issues. Wind tunnel tests are subjected to scale and tunnel interference effects while simulation models still require validation which is usually carried with reference to tunnel measurements. To this end, tunnel interference is taken into account by correcting the pitch attitude on the basis of the Glauert's and Brooks' correction methodologies. With the aim of clarifying this point, within the HeliNoVi European research project, a simulation model which also includes the tunnel interference was developed and simulations were carried out. The core model is GenUVP, a new aeroelastic code based on vortex theory which allows simulating the development of the tunnel shear layer. The model combines panel methods with vortex blob approximations for the free vorticity which is extended to the shear layer of the tunnel. The simulations are carried out in time on the full configuration demanding at every time step convergence of the non-linear aeroelastic coupling equations. In addition load trim is applied. Simulations of this type especially when the evolution of the tunnel shear layer is included require a large number of full revolutions in order to attain convergence to a periodic solution. In order to make simulations feasible, special time saving techniques are introduced in the wake. Following a similar experimental exercise, free flight results are compared with results obtained in the wind tunnel with and without correcting the angle of attack in terms of the rotor power. It follows that the correction needed closely follows the results of the experimental exercise at all speeds. Furthermore by correcting the angle of attack close correlation of the vibratory loads between free-flight conditions and operation inside the wind tunnel is confirmed. The first part of the conclusions drawn, confirms the consistency of the tunnel interference modelling while the second part reconfirms the need for reviewing and fine tuning the structural data for the particular model. Other worth noticing capabilities of the model, are the possibility of defining the best positioning of the model and of also correcting the roll angle.

1 INTRODUCTION

Over the last years wind tunnel testing of full helicopter configurations has developed into a powerful tool for the design and assessment of rotorcraft systems. As compared to flight tests,

– Wind tunnel measurements have significantly lower cost;
– Design modifications are easier to implement and therefore a quicker assessment of new concepts is possible;
– The flow conditions are well defined;
– Very detailed measurements can be obtained in all aspects: unsteady pressures, flow characteristics, deformations, structural loads, noise;
– Measurements can be used for the validation of simulation tools.

In this connection a number of projects have been carried out, most of which concern the 40% scaled BO105 helicopter (HELINOISE, HELIFLOW, HART, HeliNoVi). In certain aspects, the most recent of these projects, HeliNoVi [1], can be regarded as more complete. First the model also included the Tail Rotor while the recordings of blade deformations and flow characteristics which applied the SPR and PIV techniques are very detailed. Furthermore detailed noise measurements were also performed so in total the HeliNoVi database has a significant importance in view of evaluating and validating relevant prediction tools. In particular, one of the objectives of HeliNoVi was to assess the prediction capabilities of some prediction codes of varying complexity both with respect to noise and to vibrations. Of course the other also very important aspect was to provide further evidence that wind tunnel tests can be well correlated with flight tests.

It is well known that tunnel tests are subjected to scale and tunnel interference effects. So it is not possible to have close correlation with full scale unless proper correction actions are taken. In this connection a series of wind tunnel tests was conducted for the 40% scaled model of the BO105 helicopter in different tunnel configurations of the DNW, while the full-scale model was also measured in the NASA Ames 40x80ft closed section. A report on this exercise can be found in [2] while the main conclusions are summarized in the sequel for the sake of completeness. As regards corrections for scaling effects, it was concluded [3] that Mach scaling as expressed by the tip velocity is indispensable and the same holds for the blade per rev natural frequencies and the Lock number. Then for the Reynolds number similarity, in order to compensate for the resulting differences in air-loading the chord must be increased. For the BO105 and on the basis of the power coefficient, a 10% increase in chord is sufficient to bring the performance of the 40% scaled rotor measured in the 8x6 open test section of the DNW close to that of the full scale rotor measured in the 40x80ft NASA Ames tunnel. Given this the second point concerns the rotor trim. It is concluded that [4], the best option is to use loads trim, i.e. to match the total lift force and the MR shaft pitch and roll moments wherefrom the collective and the two cyclic pitch values are defined. Finally as regards tunnel interference, the basic idea is that the tunnel will change the effective angle of attack of the rotor which must be corrected so as to match the power. In [2] the Glauert [5] and Brooks [6, 7] methodologies were applied and evaluated based on measurements. For the 8x6m open section, the two methodologies give similar correction angles which are adequate for well correlating tunnel and flight test performance data.

Within HeliNoVi, the tunnel tests were defined with respect to flight tests and the Brooks corrections were applied. Simulations were performed with reference to the flight tests. Although predictions were found in an overall satisfactory agreement with measurements, the deviations could not be always explained. Tunnel interference was indicated as one possible explanation especially at low speeds. In order to better understand this point, a model was developed which included the wall tunnels and the free shear layer developed within the open test section of the DNW. In this connection the data reported in [2] can be regarded as basis for validating such a prediction model. In particular, these data include performance meas-

urements with and without tunnel corrections. Of course the purpose in [2] was to correlate tunnel tests with flight tests which besides the scale also concern a different helicopter. So in order to be consistent in the validation of the prediction model, one could use instead of full-scale tests, free flight simulations on the scaled model. In such an approach, the correction of the angle of attack in the wind tunnel should aim to provide the same power as in the simulated free flight.

In the present work the aeroelastic model, GenUVP (=General Unsteady Vortex Particle code) was used. GenUVP solves in the time domain the aeroelastic equations starting from rest. The aerodynamic model is based on the combination of a low-order panel method and the vortex blob approximation of the free vorticity. The solution procedure is non-linear in the sense that the non-linear aeroelastic coupled equations are solved iteratively at every time step until convergence is achieved. The fact that vorticity is modeled as a collection of freely moving fluid particles carrying vorticity allows to directly extend the method to also include the vorticity of the free-shear layer originating from the trailing edge of the inlet nozzle. This layer will develop by its self induced velocity in combination with the flow induced by the helicopter model. The simulation is continued until a trimmed periodic state is attained. A concise description of GenUVP is given in Section 2. Then in Section 3 two sets of results are presented. The first set corresponds to a summary of the comparisons made between free-flight aeroelastic simulations and measurements. The angle of attack of the MR in these simulations is obtained directly from the flight tests. They are presented with the aim to quantify the quality of predictions GenUVP can provide. The second test concerns the validation of the tunnel model and the assessment of the corrections usually made. Next in Section 4 an overall discussion is made in view of evaluating these developments and providing guidelines for future developments.

2 MODELLING CONSIDERATIONS

Modelling of the helicopter behaviour requires the solution of the aeroelastic equations, basically because otherwise trimming is questionable. Most of the existing aeroelastic tools are based on beam theory for the structural part and on potential flow theory for the aerodynamic part which quite often is even simplified to the level of lifting-line theory. Comprehensive codes and some of the research codes include blade flexibility through a chain of codes. This is an attractive approach because it allows using advanced CFD such as compressible Unsteady Reynolds Navier-Stokes solvers [8, 9]. However despite the tremendous progress of computer capabilities, it is still not feasible to run systematically aeroelastic simulations using modern CFD tools. So in order to perform cost effective simulations of full helicopter configurations, in which the aeroelastic equations are solved simultaneously, it is necessary to introduce simplifying assumptions. The model used in this work has been developed along these guidelines.

2.1 The flow modelling

For the modelling of the flow GenUVP combines a low-order panel method [10] with a vortex particle (or blob) approximation of the wake [11-13]. The theoretical backbone of the method is the Helmholtz decomposition theorem [14] according to which any flow-field $\vec{u}$ can be decomposed in a potential part $\vec{u}_{solid} = \nabla\phi$ associated to the presence of solid boundaries and a vortical part $\vec{u}_{wake} = \nabla\times\vec{\psi}$ associated to the wake or free vorticity $\vec{\omega}$ where ϕ and $\vec{\psi}$ denote the scalar and vector potentials of the flow respectively: $\nabla^2\phi = \nabla\vec{u} \equiv \Delta$ and

$\nabla^2\vec{\psi} = -\nabla\times\vec{u} \equiv -\vec{\omega}$. Then Green's theorem provides integral representations for both parts which in the case of an inviscid and incompressible flow take the following form:

$$\vec{u}_{solid}(\vec{x};t) = \int_{S(t)} \frac{(\sigma\cdot + \vec{\gamma}\times)\vec{r}}{4\pi\vec{r}^3} dD(\vec{y}) \quad \vec{u}_{wake}(\vec{x};t) = \int_{D_\omega(t)} \frac{\vec{\omega}(\vec{y};t)\times\vec{r}}{4\pi\vec{r}^3} dD(\vec{y}) \tag{1}$$

In (1) $\vec{r} = \vec{x} - \vec{y}$, $D_\omega(t)$ denotes the region covered by the wake, $S(t)$ denotes collectively the solid boundaries and $\sigma, \vec{\gamma}$ denote the surface source and vorticity distributions associated to the normal and tangent to S velocity components. By construction they both vanish at infinity so the velocity at infinity $\vec{u}_{ext}$ must be added in order to form $\vec{u}$.

Based on the above kinematic formulation, the flow equations to be satisfied are:

- The no-penetration boundary condition: $\vec{u}\cdot\vec{n} = \vec{U}_S\cdot\vec{n}$ where $\vec{U}_S$ denotes the body velocity. $\vec{U}_S$ will include the rotational speed, the speed induced by the pitch control as well as the deformation velocity.
- The vorticity emission condition also known as Kutta condition. It is applied on the solid surface at predefined lines such as the trailing edge or the tip; where from the bound vorticity is released continuously in the free flow so as to form the wake. It imposes zero pressure jump across the wake at the emission line.
- The Helmholtz equations, i.e. the momentum equations written with respect to vorticity.

In potential theory wakes are introduced as material surfaces carrying surface vorticity $\vec{\gamma}$ and not free vorticity in the strict sense. However within the context of generalized functions, surface vorticity behaves exactly as free vorticity and the same holds for line vorticity as in the case of vortex filaments. In fact for incompressible fluids local integrals of generalized vorticity such as $\vec{\omega}\delta D$, $\vec{\gamma}\delta S$ and $\vec{\Gamma}\delta\ell$ here collectively represented as $\delta\vec{\Omega}$, will generate the same type of flow while satisfying the Helmholtz evolution equations.

All existing wake models can be interpreted in this way. They differ on the choice of elements to describe the wake but most importantly on whether they assume connectivity among these elements. Connectivity is necessary in order to satisfy the fundamental requirement that vorticity is div free or else that the vorticity lines in the wake are either closed or they start and end on a solid boundary or at infinity. These requirements are by construction fulfilled when the wake is formed by means of vortex filaments or is retained as a surface. Connectivity however can generate numerical problems when the wake is excessively deformed. In order to bypass this problem, GenUVP uses freely moving vortex blobs. They are 3D point vortices equipped with core. Vortex blobs are generated at every time step in a two-steps procedure. First the wake is released in the form of surface vorticity. It is in this form that the no-penetration and Kutta conditions are satisfied. Then the convection step is carried out during which surface vorticity is integrated and transformed into vortex blobs defined by their intensities $\vec{\Omega}_P$, their positions $\vec{Z}_P$ and their core sizes ε_P:

$$\vec{\omega}(\vec{x};t) \cong \sum_P \vec{\Omega}_P(t)\zeta_\varepsilon(\vec{x} - \vec{Z}_P(t)) \tag{2}$$

where ζ_ε is the cut-off or distribution function defined over the core. GenUVP uses the cubic exponential function constructed in [15] which results in the following velocity representation:

$$\vec{u}_{wake}(\vec{x};t) = \sum_P \frac{\vec{\Omega}_P(t)\times\vec{r}}{4\pi r^3}(1-\exp(r^3/\varepsilon^3)), \quad \vec{r} = \vec{x} - \vec{Z}_P \tag{3}$$

The integration satisfies the basic invariant properties of fluid flows:

$$\vec{\Omega}_P(t) = \int_{D_P} \vec{\omega}(\vec{y};t)dD, \qquad \vec{\Omega}_P(t)\times\vec{Z}_P(t) = \int_{D_P} \vec{\omega}(\vec{y};t)\times\vec{y}\,dD \tag{4}$$

while $\vec{\Omega}_P$ and $\vec{Z}_P$ are determined by integrating in time the corresponding evolution equations:

$$\frac{d\vec{Z}_p(t)}{dt} = \vec{u}(\vec{Z}_p;t), \quad \frac{d\vec{\Omega}_p(t)}{dt} = \left(\vec{\Omega}_p(t)\nabla\right)\vec{u}(\vec{Z}_p;t) \tag{5}$$

Being unconnected, vortex blobs will generate a vorticity field which will eventually in time violate the div free requirement. There are two methods to correct this error: either by remeshing or by using the Particle-Mesh method. Fortunately the Particle-Mesh method offers additionally a substantial reduction of computational cost and it has been implemented in GenUVP. It consists of determining $\vec{u}_{wake}$ and its derivatives which appear in (6b), by solving $\nabla^2\vec{\psi} = -\vec{\omega}$ over a Cartesian grid by means of a Fast Poisson Solver [16].

In the above formulation the pressure field has been eliminated from the momentum equations when taking its rotational. By taking the divergence of the momentum equations, the pressure field can be determined by integration. In fact it turns out that the pressure will be the sum of the pressure defined by the unsteady Bernoulli equation plus an extra term due to vorticity which satisfies the following Poisson equation: $\nabla^2 p = -\nabla(\vec{\omega}\times\vec{u})$.

The loads calculated in this way neglect Ma and Re effects. In principle it is possible to also include viscous and compressibility corrections. Viscous effects can be added using boundary layer theory while compressibility can be taken into account using embedded Euler solvers. These options are implemented in the aerodynamic part of GenUVP but they still remain uncoupled with the structural part. They were however used on a strip-by-strip basis as a posteriori corrections and the results gave evidence of significant improvement especially as regards the appearance of shock waves [17]. The other, commonly applied method, is to introduce an unsteady aerodynamic model in combination with look-up tables which is what was used in the present work.

Originally the above flow modelling was used for simulating the flow around helicopter configurations. In order to also include an open jet tunnel surrounding the most important point is the free shear layer generated by the inlet nozzle. During the early stages of the present work several models were tested. A gradual development of the shear layer in the form of a vortex sheet turned out to be unstable for time steps of logical size. The starting vortex rolls-up into a vortex ring which until it reaches the collector generates large deformations on the shear

layer. In order to bypass this problem, it was assumed that the simulation starts when the flow in the tunnel has fully developed. So at t=0, the complete shear layer was embedded in the flow simulation. It consists of a vortex sheet connecting the inlet nozzle and the collector which are also present in the simulation. The shear layer is represented in the form of vortex blobs which are left to evolve freely. At every time step a new series of vortex blobs are released along the edge of the nozzle and at the same time the last series is absorbed by the collector. Otherwise the shear layer itself is free to evolve and adjust its shape according to the local flow. The intensity of the shear layer along the emission line of the inlet nozzle is set equal to the reference tunnel speed of each case.

In the absence of any model in the tunnel flow, it is expected that the flow should be approximately uniform (Figure 1). Physically consistent results were also obtained when a sphere was introduced (Figure 2). Another point which was also checked is the effect of the walls of the closed chamber. Numerical tests showed that within the measuring region there were no appreciable differences and therefore they were not finally retained. This is necessary compromise if systematic runs are to be carried out because the additional charge in run time is significantly greater.

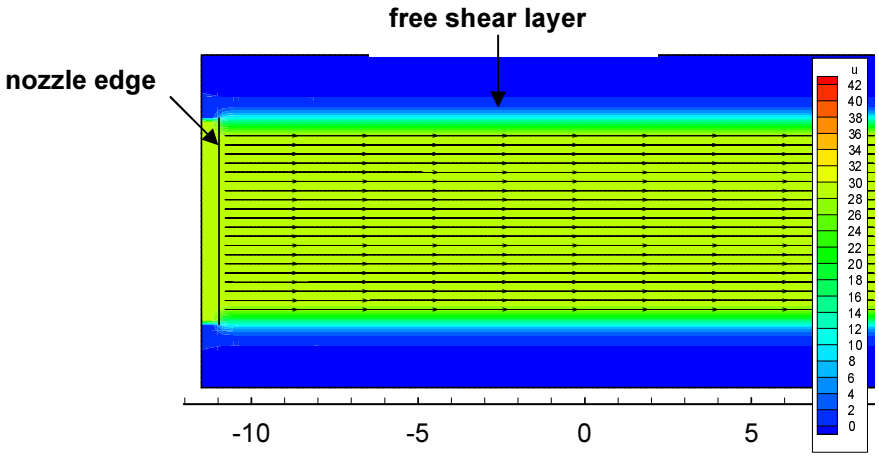

Figure 1: Generation of the wake and formation of vortex blobs (Reference speed 30 m/s).

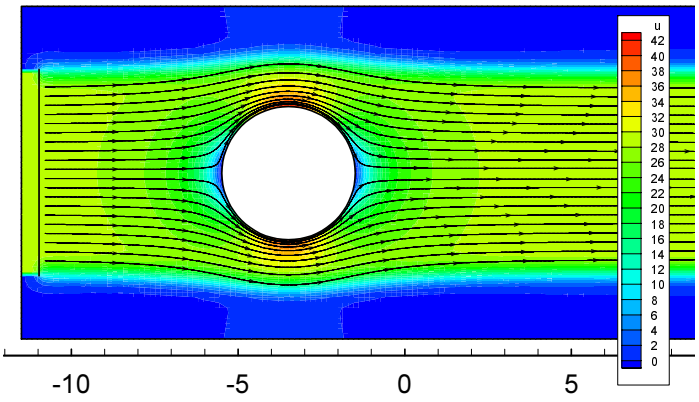

Figure 2: Generation of the wake and formation of vortex blobs (Reference speed 30 m/s).

2.2 Modelling of the dynamics

GenUVP models the blade flexibility using the 2nd order beam model of Hodges and Dowell [18] in the context of the Finite Element Method. The blade is considered in its deformed state and therefore the solution is carried out iteratively. Because the aerodynamic loads originate

from a potential flow solver, there is need to introduce an unsteady aerodynamics model in order to account for Ma and Re effects. To this end the ONERA model is employed in its generalized formulation written with respect to generalized circulation parameters $\Gamma_{1L}, \Gamma_{2L}, \Gamma_{2D}$ and Γ_{2M} [19]. The specific formulation fits well in the overall framework of GenUVP as it allows a direct link with the 3D aerodynamic model. In particular the attached part of lift Γ_{1L} is directly taken from the 3D computations. For the other components, model 2nd order dynamic equations are solved. Otherwise the model uses look-up tables based on the 2D steady polars which were provided as part of the BO105 wind tunnel model database [20].

The beam structural model is introduced into the dynamics model which is based on a multi-body formulation which in the case of a helicopter configuration allows introducing in detail the hub characteristics together with the controls and eventually existing rigid body motions. In multi-body modelling each component *k* is assigned a local coordinate system O*xyz* with its undeformed elastic axis along the *y* axis. Then the position of a point with respect to the fixed system $\mathbf{r}_{G,k}$ can be expressed with respect to its local position as follows:

$$\mathbf{r}_{Gk} = \boldsymbol{\rho}_k + \mathbf{A}_k \cdot \mathbf{r}_k \tag{6}$$

where $\boldsymbol{\rho}_k$ denotes the position of the origin of the local system with respect to the fixed system and $\mathbf{A}_k$ denotes the local to global transformation matrix. The above expression is used in defining the inertia loads. The exact form of $\boldsymbol{\rho}_k$ and $\mathbf{A}_k$ depends on the kinematic conditions introduced when connecting the various components (e.g. the blades-to-hub or pitch link). Depending on the type of connection, common global displacements and rotations are assigned for the restricted d.o.f., which are identified to either an existing elastic d.o.f. (shaft bending at the hub) or a rigid body motion (blade pitch). The component contributing the kinematics will in response receive from the rest of the connected components their internal (or reaction) loads. This operation involves co-ordinate system transformations between the components. The set of kinematic degrees of freedom involved in the definition of $\boldsymbol{\rho}_k$ and $\mathbf{A}_k$ for all components is denoted collectively as $\mathbf{q}$. So $\boldsymbol{\rho}_k = \boldsymbol{\rho}_k(\mathbf{q};t)$ and $\mathbf{A}_k = \mathbf{A}_k(\mathbf{q};t)$. $\boldsymbol{\rho}_k$ is defined as a mixed series of translations and rotations, whereas $\mathbf{A}_k$ is defined solely as a sequence of rotations. By construction $\boldsymbol{\rho}_k$ and $\mathbf{A}_k$ will depend on unknown d.o.f. while at the same time they correlate the state of the components in contact so the terms they generate are non-linear with respect to the unknown d.o.f.. In GenUVP the exact expressions are implemented and the solution is obtained through an iterative procedure in each time step.

3 RESULTS

The results presented in this paper are organized in two groups. The first group concerns simulations of the complete configuration performed in free-flight conditions with the Main Rotor angle of attack taken from flight tests. Predictions are compared to measurements with the aim to assess the accuracy of GenUVP in its full form. The second group concerns simulations specifically performed in view of assessing the tunnel model as well as the tunnel corrections which were used within the validation activities of the HeliNoVi project.

3.1 Validation of GenUVP

The validation task within HeliNoVi scanned a wide range of aspects including unsteady surface pressures, aerodynamic loads, deformations, structural loads, flow characteristics and

noise. In concise form they are reported in [21, 22] (for a full account see [17, 23-25]). In this paper a summary of representative results are shown which can judge the quality of predictions GenUVP can provide.

Figure 3 shows the azimuth variation of the normal force coefficient at the r/R=0.87 radial section for two level flights at 33 and 60m/s and a descent flight at 33m/s. In general there is good agreement with the measured data especially for the descent case where the BVI encounters are well predicted. Over the 2nd quadrant for the two level flight cases, the loss of loading seen in the measurements is not captured. Because the loss of loading takes place also at low flight speed for which compressibility effects are not expected to be as important, the difference has been attributed to the poor capturing of the tip vortex evolution as a result of the relatively large time step. The tip vortex over this particular quadrant is expected to roll-up over the blade as a result of the radial flow basically introduced by the incoming flow. Such a roll-up will degrade locally the effective angle of attack and consequently the lift. In order to capture this kind of detail, if possible, a much smaller time step should had been used (these particular runs were performed with 90 steps per period). A similar effect is seen over the 4th quadrant, predicted this time in the opposite sense. It is noted that as the flight velocity increases the time step required in order to capture this roll-up would decrease. Another point concerns the 1st quadrant for the level flight at 60m/s, over which predictions underestimate the loading. This is attributed to compressibility effects which would cause the appearance of shock waves. When the Euler solver was used, it was possible to see these effects as shown in Figure 4. As a result of the increasing differences in the blade aerodynamic loads with the flight speed, due to the Ma number effect, the lateral component of the cyclic pitch is under estimated at higher speeds (Figure 3).

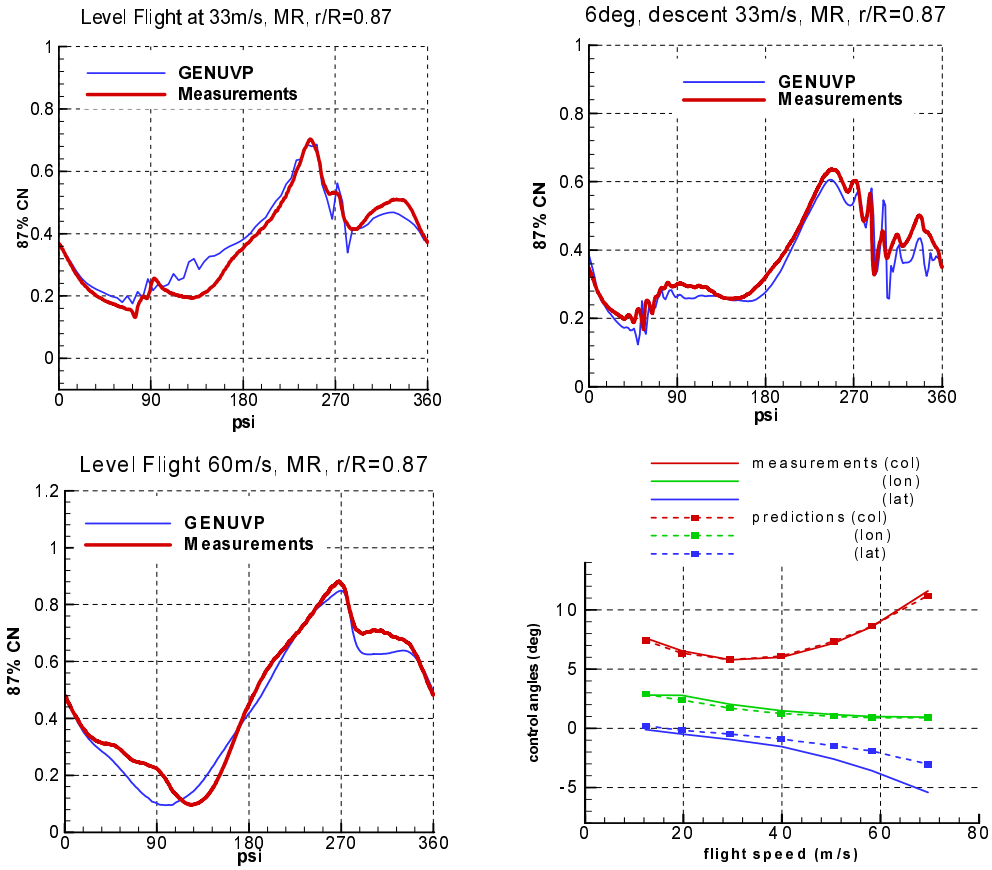

Figure 3: MR CN azimuth variation & control angles versus flight speed.

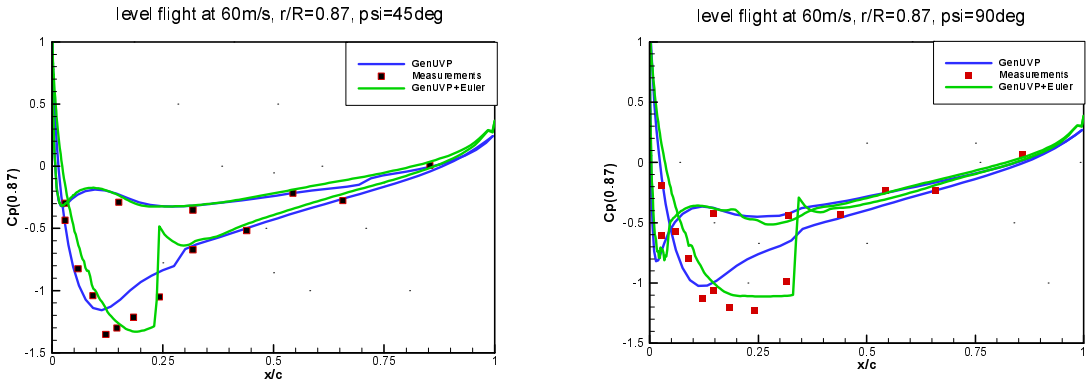

Figure 4: Cp distributions over the 87% radial station at azimuth angles 45° and 90° for a level flight at 60m/s

Next comparisons with respect to the structural characteristics are shown in terms of blade deformations and loads. Measurements from one blade and one sensor will be shown, although sensors were placed at all blades and at different locations. As usually there was scatter in the measured data which is not shown here.

Figure 5 shows the tip deformations for a level flight at 50.9m/s. The flap deflection is in fair correlation with respect to measurements. While the amplitude is correctly predicted, there is a difference in the frequency response. The measurements indicate almost equal excitation of the 2/rev and 3/rev harmonics while in the predictions 3/rev component almost vanishes. In the lag direction, measurements appear to be offset with respect to predictions (this was found in all flight conditions). This offset corresponds to a rigid body rotation performed by the blades probably due to the compliance/flexibility of the drive train system and/or the hub. In the simulation the drive system and the rotor hub are considered infinitely stiff. This explains the much lower deflections obtained with respect to measurements. Besides the difference in the mean blade deformation, the 1/rev variation of the lead-lag motion is well predicted. The high frequency oscillation seen in the measurements corresponds to the response of the blade to its 2nd lead-lag natural frequency. This response appears to be significantly weaker in the calculations. The highest deviations are obtained in the torsion angle. The predicted tip torsion angles are shifted in phase as compared to the measured ones. This phase shift is attributed to the modelling of the hub, which has been assumed rigid. Near the blade root, predictions give almost zero torsion deflections while the measured angles have already quite high values [25], indicating that the hub of the model rotor is not rigid. Otherwise both measurements and predictions agree that the torsion angle is dominated by a 1/rev variation. Also, in accordance with the results shown for the flap displacements, the predictions underestimate the 3/rev component of the torsion angle variation.

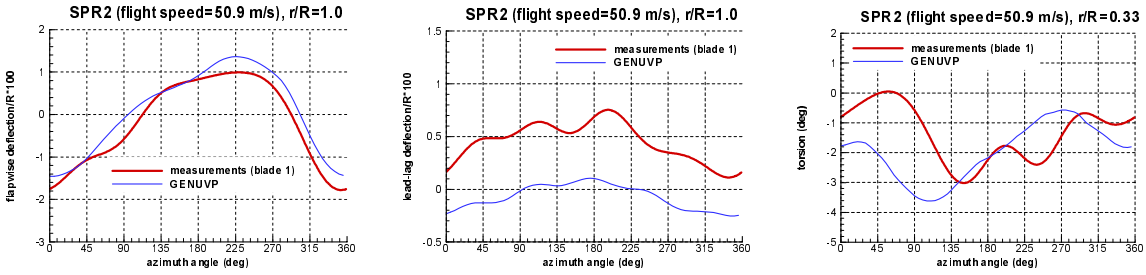

Figure 5: Azimuth variation of the tip deformations in level flight at 50.9 m/s

Figure 6 shows the mean values of the flap moment at r/R=0.1465, the lag moment at r/R=0.0300 and r/R=0.1440 and the torsion moment at r/R=0.33 versus the flight speed. Two sets of predictions are presented with and without the fuselage. In these plots the basic remark is that good correlation with measurements is obtained in the torsion moment while level differences are noted in the other two loads, smaller in the lead-lag moment at r/R=0.0300 (sensor located on the hub arm) and higher in the flap moment. The higher level difference seen in the lead-lag moment at r/R=0.1440 (sensor located on the airfoil) is due to the sensitivity of the results to the location of the sensor along the blade chord. In the flap variations there is also some deviation in trend at low speeds, while the introduction of the fuselage does not affect the results. The level difference seen in the flap and lag are attributed to the structural data used in the simulations. The blade data were taken from a former data set which in principle should correspond to the data of the particular blades. Also the hub and the controls were assumed perfectly rigid which is not justified by the measurements.

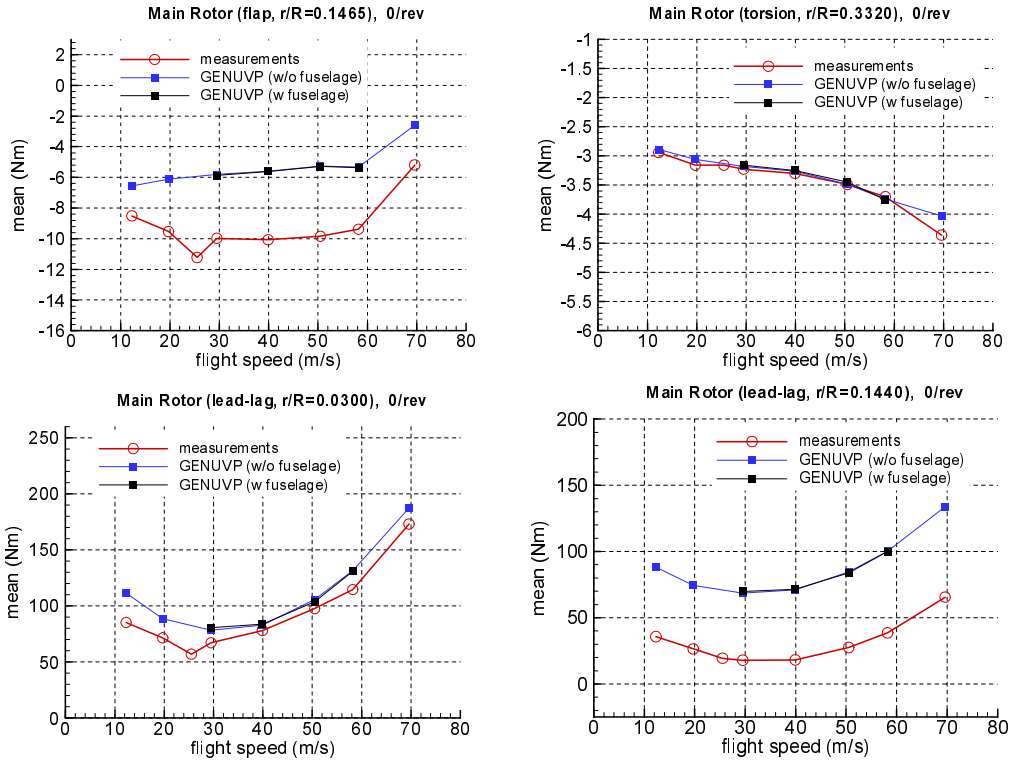

Figure 6: Azimuth variation of the mean structural moments versus flight speed

Figure 7 gives the variation of the 3/, 4/ and 5/rev components of the three moments versus the flight speed. The predicted 3/rev variations have the same overall behavior as in the measurements. There is a consistent underestimation in flap results which gets more pronounced over the intermediate flight speeds. By introducing the fuselage, an improvement is obtained which however does not shift the curve uniformly. As regards the 4/rev variations the correlation is mixed. For the flap moment, predictions have the same behavior as for the 3/rev while for the lag and torsion moments the predicted trend is different. The introduction of the fuselage leads to smaller improvement. For the lag moment, there is level shift which as explained in the sequel, is attributed to differences of the structural model as compared to the actual characteristics of the measured blade. For the torsion moment, there is agreement in the level but not in the trend. Finally as regards the 5/rev predictions, for the flap and torsion moments the level of values match those measured. However the trend in the variation of the flap is different getting maximum in the measurements at the lowest speed while dropping in the predictions. For the torsion moment the variation is relatively good. For the lag moment the

simulation shows higher excitation and different trend. The high 5/rev lag amplitudes in the simulations are connected to the response of the blade to its 2nd lead-lag natural frequency, which in the case of the tested blade is probably shifted to lower values lying more closely to the 4/rev. So, this difference can be attributed to the differences in the structural data.

Figure 8 shows the variation of the 4/rev component of the roll and pitch hub moments. They are both dominated by the 3/rev harmonics of the flap, and this is consistently reproduced by GenUVP. The differences seen already in the blade flap loads are clearly reflected on the mast loads. The introduction of the fuselage increases the hub loads at moderate speeds and improves the correlation with the measurements:

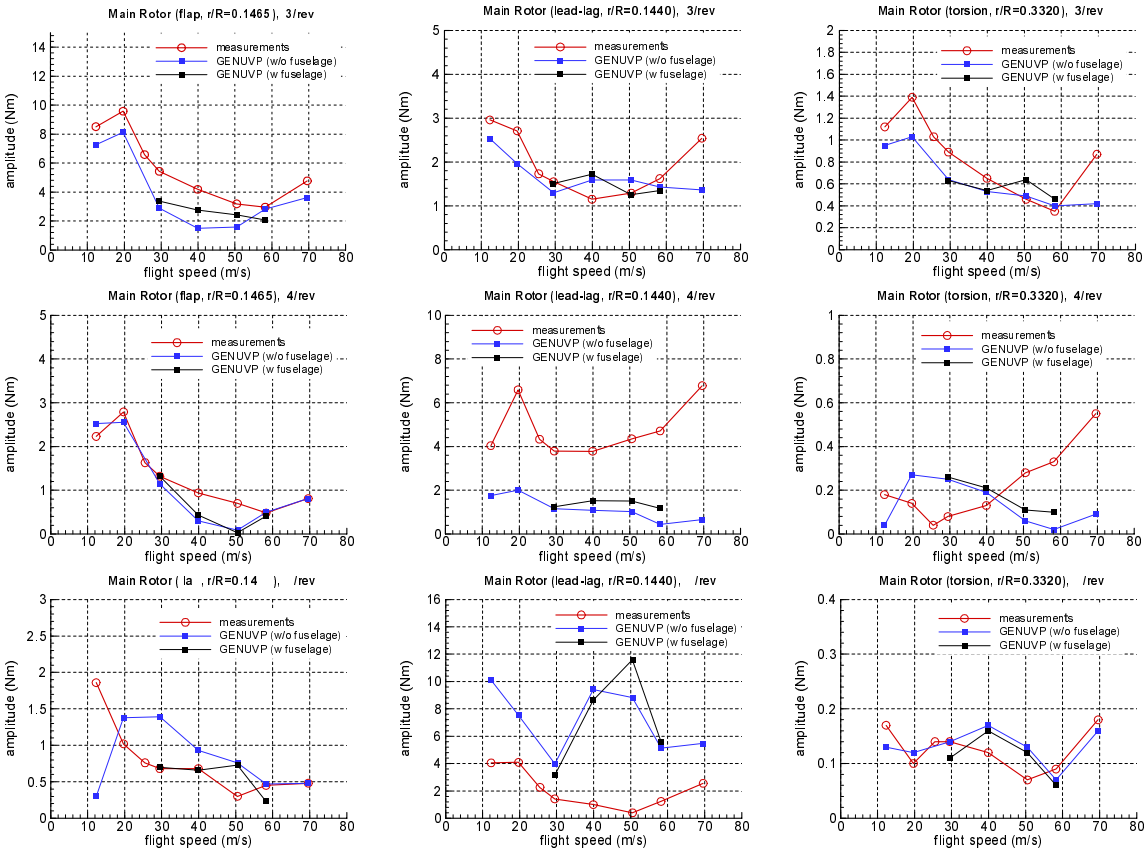

Figure 7: Variation of the 3, 4 and 5/rev harmonic of the flap, lag and torsion moments versus flight speed.

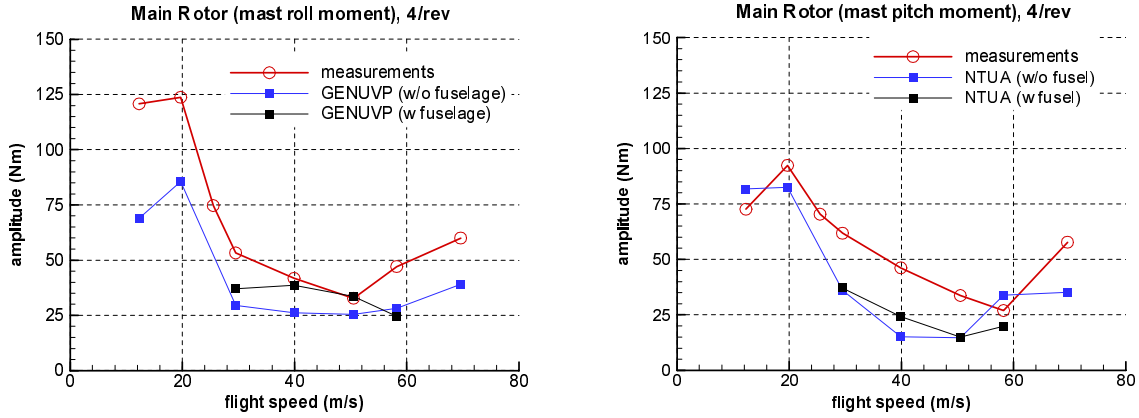

Figure 8: Variation of the 4/rev roll and pitch moments versus flight speed

Finally the last result concerns the flow field over the rotor disk. In Figure 9 predictions are compared to PIV measurements over the retreating side of the rotor for a flight speed of 50.9m/s. In the measured data, the rotor blades and the streaklines of the tip vortices have been added in order to facilitate the comparison. Overall there is good agreement. The presence of the blades is clearly shown while the distortion induced on the flow is well captured. The same holds for the tip vortices. The blade in the measurements appears to lag in position. Since a similar shift is seen also for the positioning of the trailing vortices it follows that this is probably due to some offset in the time recorder. Of similar quality were all the comparisons reported in [25].

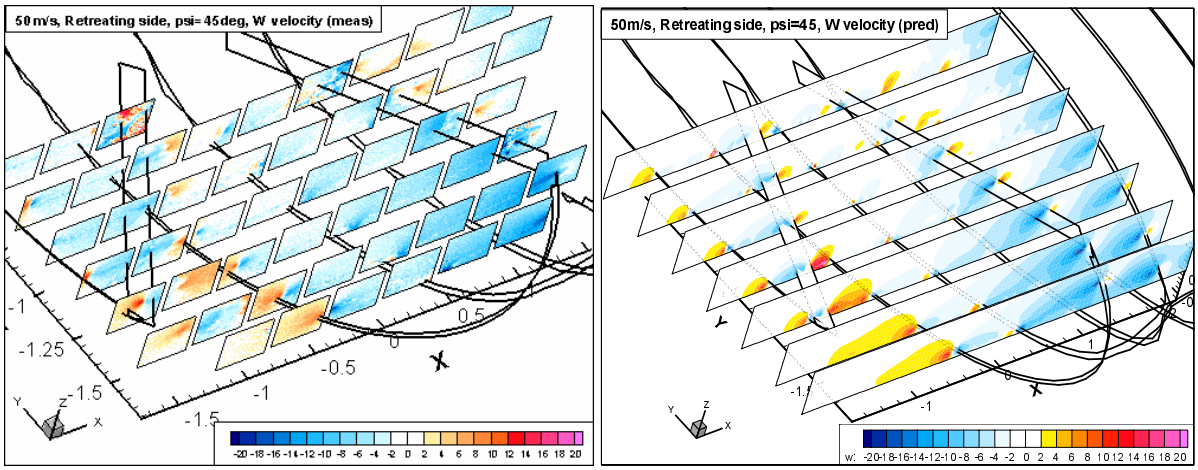

Figure 9: Comparison of the measured (left) and predicted (right) W component contours over the retreating side at psi=45deg (50m/s)

3.2 Validation of the tunnel model and assessment of the tunnel corrections

The simulations concerning the tunnel model were performed with only the MR in order to reduce the total computational cost of this investigation. Depending on the flight speed, the cost of the simulation in free-flight conditions varies from 5 to 15 days on a single processor corresponding to a total of 50-60 MR rotations. This is basically due to the fact that the full aeroelastic model is run from the beginning of the simulation.

In Figure 10 the layout of a typical simulation is shown. It corresponds to the 8x6 open jet configuration of the DNW wind tunnel. The distortion of the tunnel shear layer caused by the presence of the rotor is clear. A more quantitative representation of the effect the tunnel has on the flow is shown in Figure 11 where the free-flight case is compared with that in the tunnel for a flight velocity of 20 m/s. Note that the rotor shaft angle in the tunnel is different and corresponds to the correction made in order to match the two conditions. The contours in both figures represent the horizontal flow velocity.

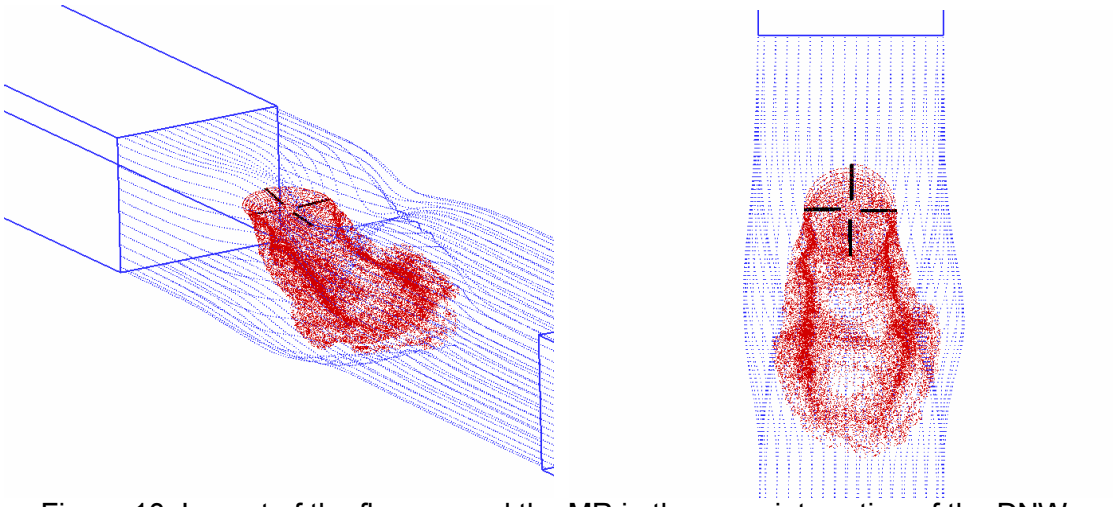

Figure 10: Layout of the flow around the MR in the open jet section of the DNW.

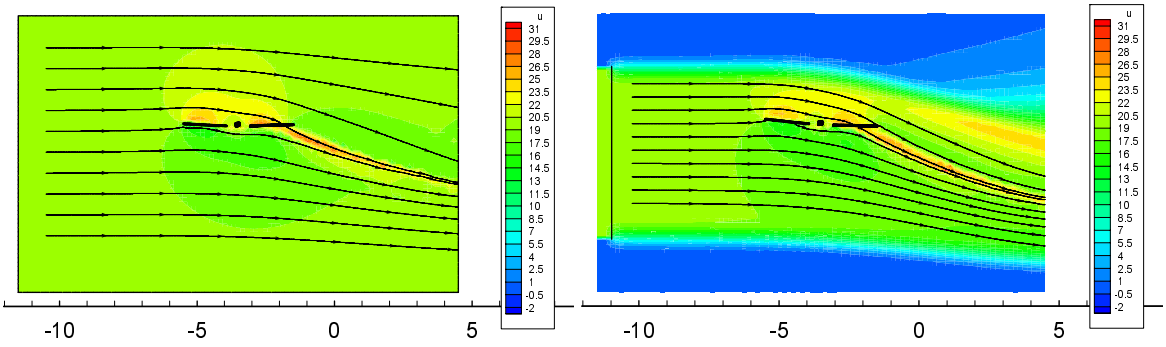

Figure 11: Layout of the flow around the MR in free flight (left) and in the open jet section of the DNW (right) at 20 m/s.

The test matrix of simulations included 5 flight speeds in forward flight conditions, at 20, 30, 40, 50 and 60m/s. For each flight speed three simulations were performed: a free-flight simulation, a simulation in the tunnel with the same rotor shaft angle (baseline) and a simulation in the tunnel at the corrected angle of attack (corrected), as provided by Brooks method. The rotor in all cases was trimmed for given thrust and mast moments according to flight-test data. The above approach closely follows the methodology used in [2]. There are however some differences. In [2] the trim was based on the total lift which also includes the force on the fuselage. Also the assessment of the tunnel corrections was carried out with respect to the rotor power and the propulsive force, while in the present work, only the rotor shaft torque was considered. Since the fuselage was not included[1], trimming for given thrust and the same pitch attitude, will also match the propulsive force provided by the MR. Despite these differences, the data reported in [2] can be used for validating the tunnel model by comparing the change in power obtained by changing the angle of attack. The rotor system used in [2] is the same with that of HeliNoVi and so holds for the thrust coefficient and the tunnel set up.

Figure 12a, shows the predicted variation of the rotor power coefficient with respect to the flight speed while for the sake of comparison the experimental results reported in [2] are shown in Figure 12b. Correcting the rotor shaft angle, based on Brook's, is sufficient to almost match the tunnel results with those in free flight. By comparing the predicted changes in C_P with those measured, a close agreement is found at all advance ratios.

[1] It is noted that even if the fuselage were included in a potential flow context, the result would had been the same. In this case the use of a viscous solver is indispensable.

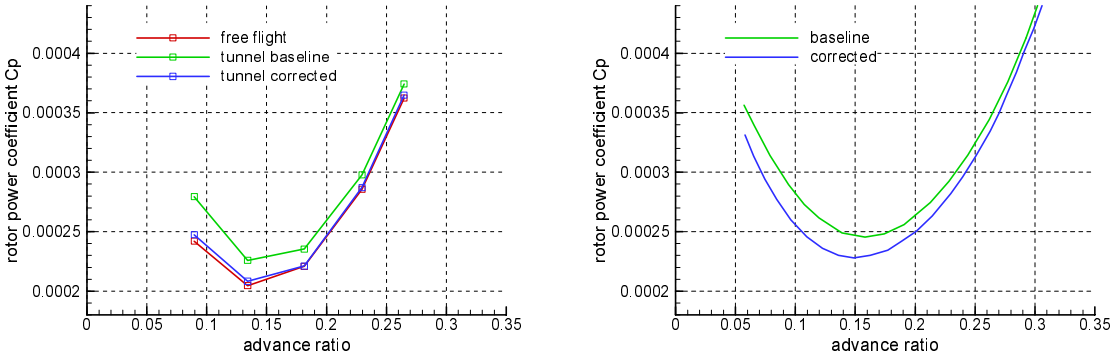

Figure 12: Predicted C_P variation versus flight speed (left) and measured C_P variation versus flight speed from [2].

In Figure 13a, the rotor shaft angle of the flight tests is plotted against those resulting by applying Brook's correction and the correction found using the present model. The corresponding correction angles for the different flight speeds are obtained as the difference of the corrected shaft angles and the flight test angles. The correction angle of the present model was estimated by extrapolating the power coefficients of the tunnel simulations to the power coefficient of the free-flight simulation, assuming linear dependency of the rotor power on the rotor shaft angle [2]. The two corrections are identical for the high flight speeds while at the two lower speeds there is a small difference. Looking into the collective pitch angle (Figure 13b), it follows that the change in angle of attack forces the collective pitch angle to move to the free-flight values. On the contrary the cyclic pitch components do not match as well (Figure 14a). In particular the longitudinal component remains shifted compared to the free-flight data which is reflected on the side force (Figure 14b). This indicates that it is possible to also trim the side force by correcting the roll attitude of the helicopter in the tunnel.

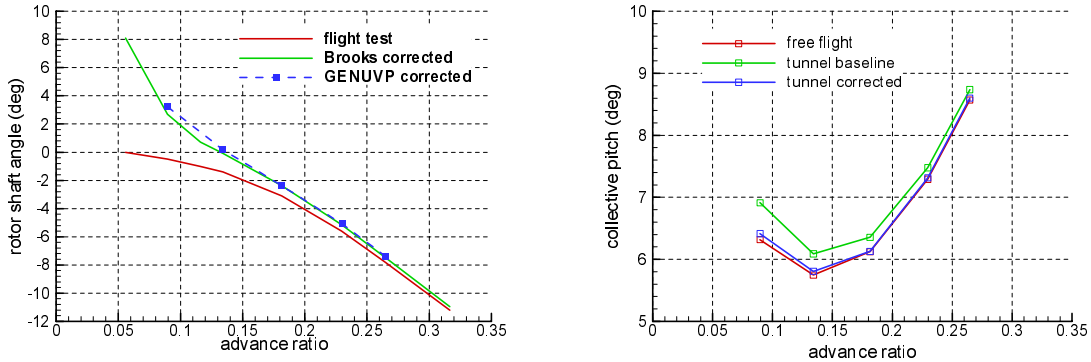

Figure 13: Variation of the angle of attack (left) and of the collective pitch angle (right) versus flight speed

Next results are presented concerning the structural loads. Figure 15-Figure 17 show the 3/, 4/ and 5/rev harmonics of the blade flap, lag and torsion moments. In the plots the free-flight results are compared with those of the wind tunnel simulations for the baseline and the corrected rotor shaft angles. Overall, the application of the correction angle in the tunnel simulations improves the correlation with the free-flight results in all flight speeds. In the flap loads and by using the baseline values of the rotor shaft angles, higher 3/ and 5/rev amplitudes are obtained at moderate and low speeds as compared to free-flight conditions. Application of correction angle brings the amplitudes to the same level with the free flight results, except for

the case of the lowest flight speed where slightly higher amplitudes are obtained. In the lag moment differences are noted in the dominant 5/rev harmonic where again the use of the baseline angles gives rise to higher loads especially at the 20m/s flight speed. As in the flap bending moment a good correlation with the free-flight results is attained when the correction angle is applied. Similar behavior is also seen in the torsion moment where again application of the correction improves the correlation with the free-flight results.

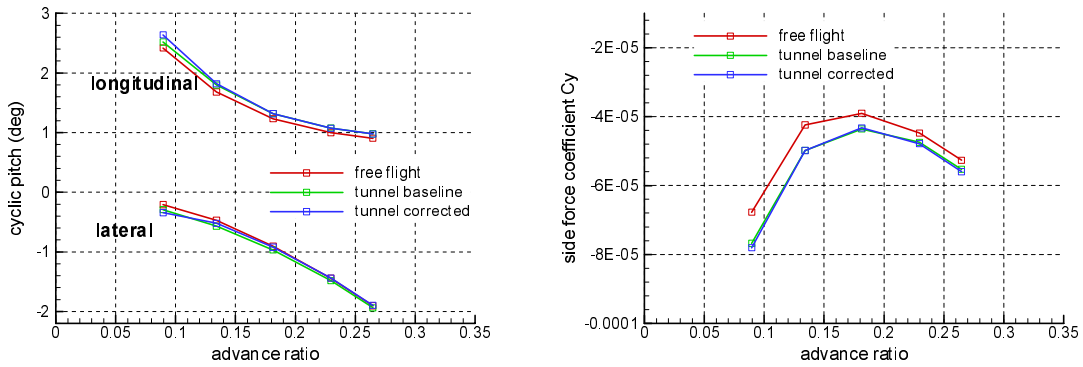

Figure 14: Predicted variation of the cyclic pitch components (left) and of the side force (right) versus flight speed.

In Figure 18 the 4/ and 8/rev harmonics of the rotor mast bending loads are presented. As already said the 4/rev amplitudes of the non-rotating hub loads are essentially dominated by the 3/rev component of the blade flapwise bending loads. In connection to that, the 4/rev harmonic of the mast bending loads is found to be higher at moderate and low flight speeds, as compared to the free flight conditions, when no correction is applied. However, in accordance with the flap results introduction of the correction leads to a very close correlation with the free-flight results. Good correlation with the free flight conditions is also noted in the 8/rev harmonic although the amplitudes of the 8/rev response are quite smaller compared to 4/rev.

4 DISCUSSION

A vortex model of an open jet wind tunnel configuration was presented. Coupled with the GenUVP aeroelastic code offers the possibility of simulating wind tunnel tests of helicopter configurations. The tunnel model was first checked for consistency and then indirectly validated with respect to the experimental results reported in [2]. In the first set of results the GenUVP in free-flight conditions was validated against the HeliNoVi experimental data base. From this part the following conclusions can be drawn:

a) With reference to aerodynamic pressure data, the predictions were found overall in good agreement with the measurements. Over the advancing side when compressibility effects become important, the use of simple corrections such as that of Glauert's or the use of look-up tables based on 2D steady polars were found insufficient to capture the loading variation (1st quadrant). It is noted that a poor approximation of the compressibility effects will reflect on the trim which was also noted. Also the simulated CN variations over the 2nd and 4th quadrants were found in level difference with respect to measurements. They were associated to the evolution of the tip vortex roll-up which in the advancing side moves over the blade and thus lowers the effective angle of attack, while in the retreating side is shifted outside the blade and thus increases the loading. The time scale of this evolution is small and therefore in order to predict it, at least a much smaller time

step must be used while viscous and unsteady compressibility effects could also have an important contribution.

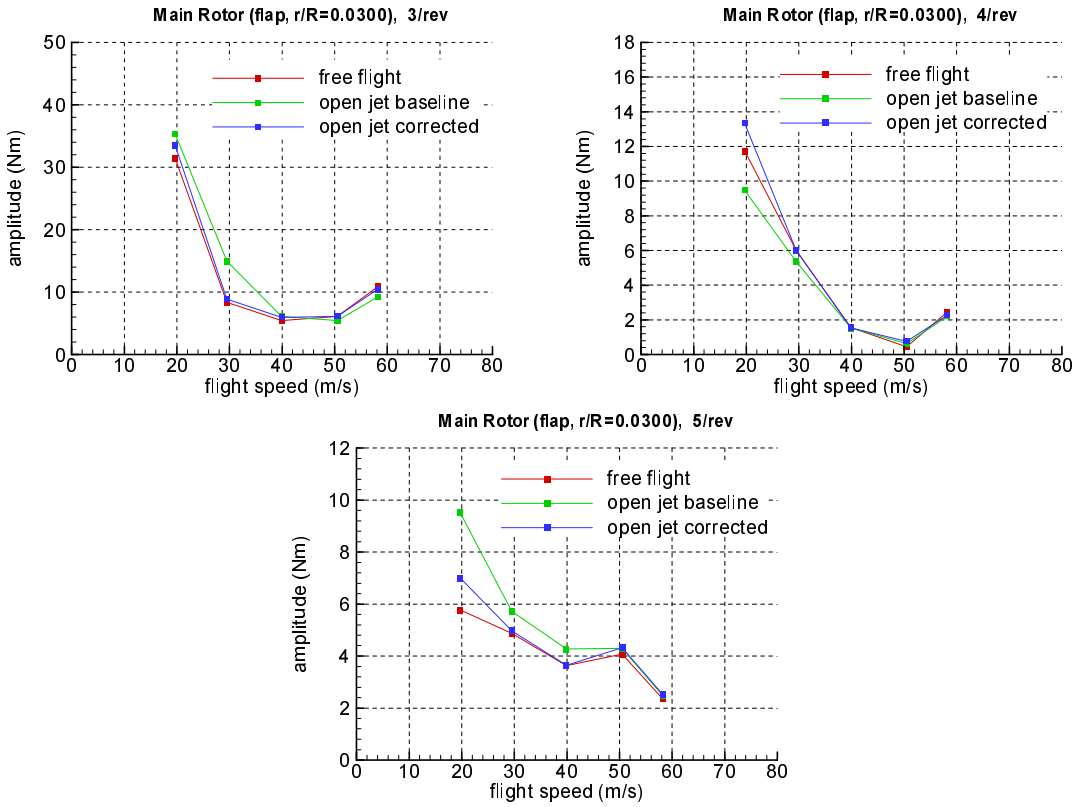

Figure 15: Harmonics of the flap bending moment versus flight speed

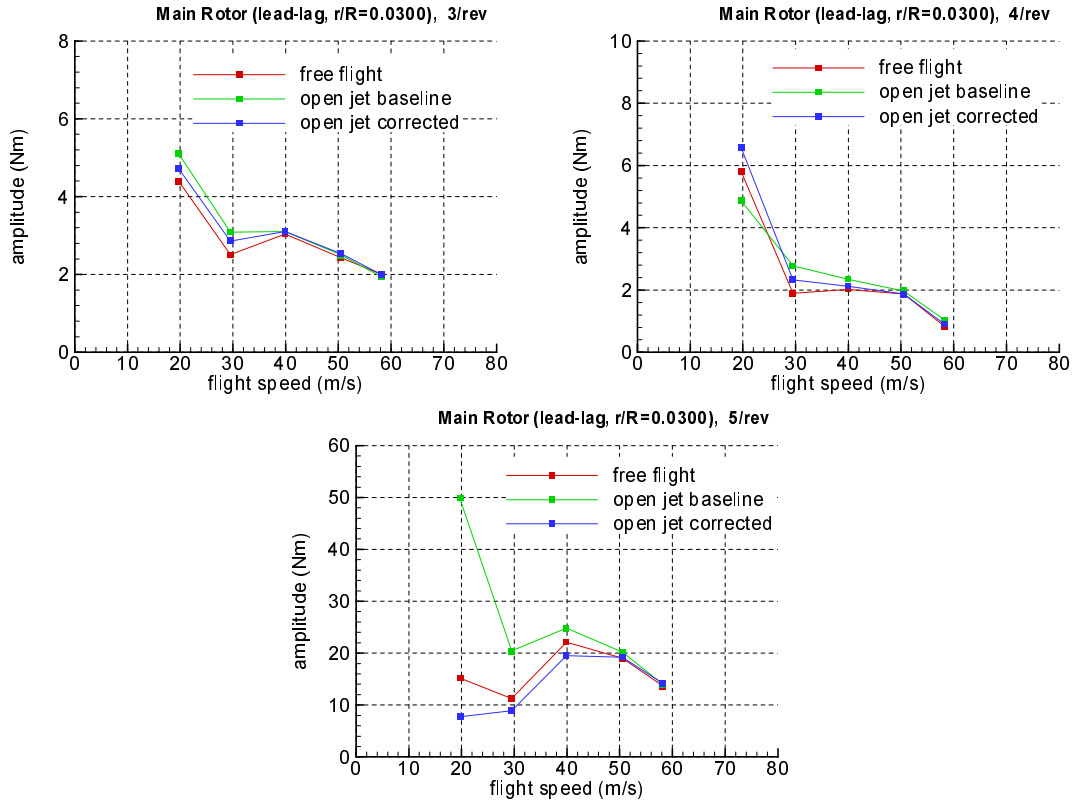

Figure 16: Harmonics of the lag bending moment versus flight speed

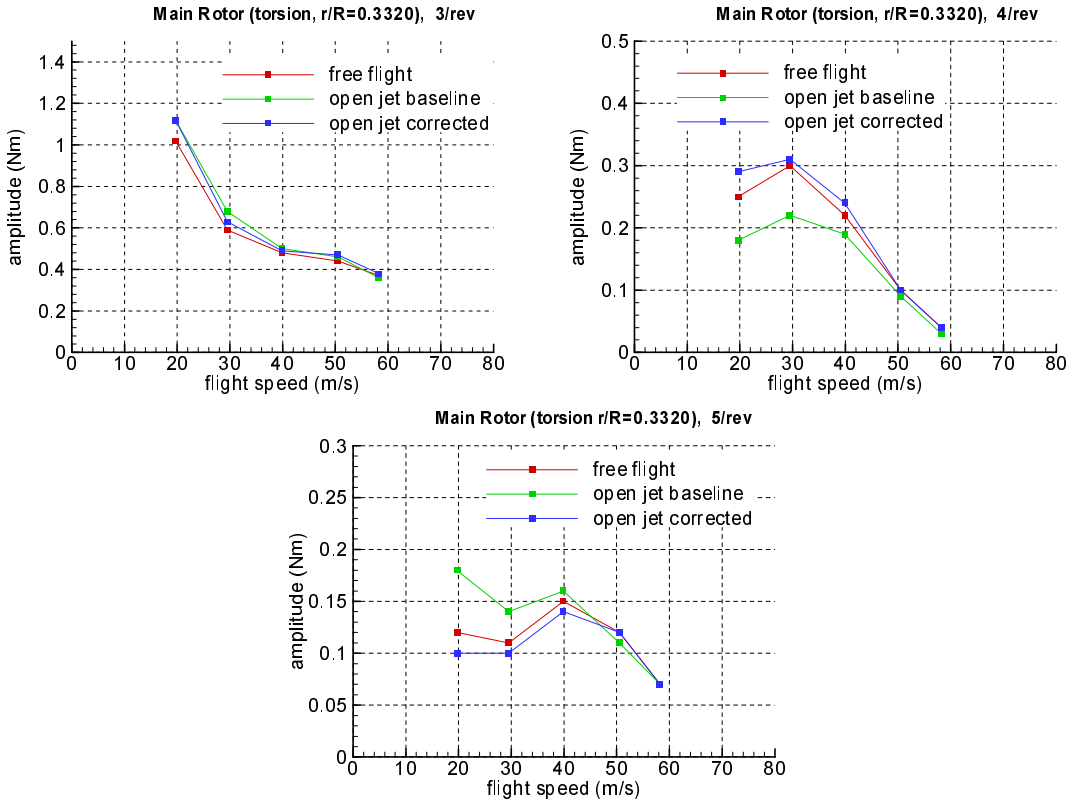

Figure 17: Harmonics of the flap bending moment versus flight speed

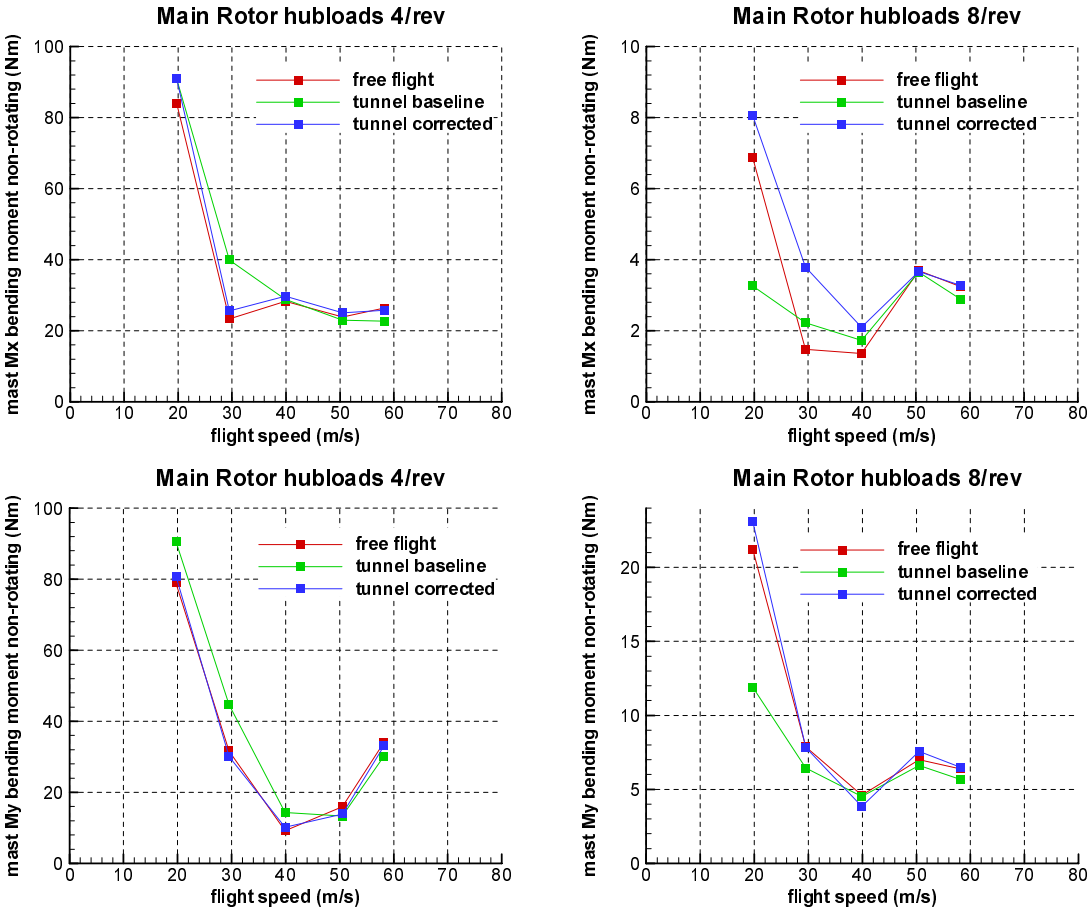

Figure 18: 4/ and 8/rev hub loads versus flight speed

b) As regards the structural response, it is important to note the particular importance of the trim and of the input structural data. As already mentioned at higher speed the predicted lateral cyclic deviates from measurements as a result of poor resolution of the Ma effects. Besides that comparisons of predictions and measurements indicated that the structural data for the blade as well as the assumption of a rigid hub and of rigid controls are not compatible with the overall characteristics with the wind tunnel model. The more pronounced excitation of the 5/rev lag moment in the simulations instead of the 4/rev excitation in the tests on one hand and the differences in the torsion angle are supportive to this conjecture. Another indication is the better correlation between predictions and flight tests reported in [26] by ECD. Another important point is the approximation of the unsteady aerodynamics which is carried out in GenUVP through the ONERA model. As shown in [25] the modeling of the unsteady aerodynamics plays a decisive role on the prediction of the structural loads. Of course any semi-empirical model of the ONERA type always depends on the set of constants used and therefore one can expect to improve predictions by specifically calibrating them. In connection to the specific comparisons made, it follows that an overall good agreement has been achieved in spite of the input data issues and the errors generated by the aerodynamic predictions. It is true that the structural loads are affected by the overall aeroelastic coupling and thus accumulate all errors or differences in the modeling.

In the second set of results GenUVP was used including the tunnel model. From this part the following conclusions can be drawn:

a) From a practical point of view, the conclusions of the experimental campaigns reported in [2] were confirmed. In particular, it follows that by changing the angle of attack of the model in the wind tunnel, it is possible to well correlate wind tunnel and flight tests. Also the corrections produced by the Brook's model have been confirmed. Of importance is also the fact that not only the performance characteristics match but also the vibration response. This means that the tunnel has an overall effect on the helicopter while the details are determined by the model itself.
b) In the particular exercise only the MR was considered. For the higher flight speeds, such a simplification should not have an important effect. However at low speeds the correction is substantial and so depending on the geometry of the configuration (size of the fuselage, rotor plane clearance with respect to the fuselage roof etc.) the effect of the fuselage should be checked. Another aspect which was not addressed in the present work, concerns the TR. The numerical flow visualizations indicate that the downstream evolution of the MR is the part most affected by the tunnel. Therefore one should check to what extent the operation conditions of the TR are affected. It is not expected that the vibration response will significantly change. The same does not necessarily hold for the TR noise which in level flight constitutes the main contribution.
c) In [2] as well as in the present work, the roll attitude of the helicopter was fixed leading to differences in the side force. In this connection it is possible to also correct the roll angle. Eventually a correction of this type could improve the trim and therefore further improve the correlation with flight tests.

5 ACKNOWLEDGEMENTS

This work was partially funded by the European Union in the framework of the Competitive and Sustainable Growth Programme under the HeliNoVi project, Contract Number G4RD-CT-2001-40113

6 REFERENCES

[1] DLR, "HeliNOVI – Annex I: Description of Work", September 2001

[2] H-J. Langer, R.L. Peterson, T.H. Maier, "An experimental evaluation of wind tunnel wall correction methods for helicopter performance", 52nd AHS Annual Forum, Washington D.C., 1996

[3] C.N. Keys, M.A. McVeigh, L. Dadone, F.J. McHugh, "Considerations in the estimation of full scale rotor performance from model rotor test data", 39th AHS Annual Forum, St. Louis, 1983

[4] R.L. Peterson, T.H. Maier H-J. Langer, N. Trahapp, "Correlation of wind tunnel and flight test results of a full-scale hingeless rotor", AHS Aeromechanics Specialist Conference San Francisco, CA, 1994

[5] A. Pope, J.J. Harper, "Low_speed wind tunnel testing", John Wiley & Sons, Inc., 1966

[6] T.F. Brooks, C.L. Burley, "A wind tunnel wall correction model for helicopters in open, closed amd partially open rectangular test sections", NASA TM, 1996

[7] P. Beaumier, C. Tung, R. Kube, T.F. Brooks et al, "Effect of higher harmonic control on helicopter rotor blade-vortex interaction noise: prediction and initial validation", AGARD Conference Proccedings No 552: Aerodynamics and Aeracoustics of Rotorcraft, paper 26, 1994

[8] J. Sitaraman, A. Datta, J. Baeder, I. Chopra, "Counpled CFD/CSD prediction of rotor aerodynamic and structural dynamic loads for three critical flight conditions", 31st ERF, Florence, 2005

[9] K. Pahlke, "The 6-year French-German CHANCE Project", 31st ERF, Florence, 2005

[10] J.L. Hess, "Calculation of potential flow about arbitrary three-dimensional lifting bodies", McDonnell Douglas Rep., MDC J5679-01, 1972.

[11] C. Rehbach, "Calcul d'ecoulements autour d'ailes sans epaisseur avec nappes tourbillonnaires evolutives », Recherche Aerospatiale 2:53-61, 1973.

[12] G-H Cottet, P.D. Koumoutsakos, "Vortex methods: Theory and Practice", Cambridge University Press, 2000

[13] S.G. Voutsinas, "Vortex methods in aeronautics: How to make things work", Int. J. Comp. Fluid Dynamics, Vol. 20, 3-18, 2006.

[14] S.M. Richardson and A.R.H. Cornish, "Solution of three dimensionsl incompressible flow problems", J. Fluid Mechanics, Vol 82, 309-319, 1977

[15] J.T. Beale and A. Majda, "Higher order accurate vortex methods with explicit velocity kernels", J. Comput. Phusics, Vol 58, 1985

[16] S. Huberson and S.G. Voutsinas, "Particles and grids", Computers & Fluids, 31, 607-625, 2002

[17] A. Visingardi "Final Validation Report of the Aerodynamic Prediction Codes", HeliNOVI deliverable D1.4-2, March 2006

[18] D.H. Hodges, and E.H. Dowell, E.H., "Non-linear Equations of Motion for the Elastic Bending and Torsion of Twisted Nonuniform Rotor Blades", NASA TN D-7818, 1974

[19] D. Petot, "Differential equation modeling of dynamic stall", La Recherche Aerospatiale 1989, 5, 59-72

[20] O. Dieterich "Wind Tunnel Model Database", HeliNOVI deliverable D2.1-1, September 2002.

[21] A. Visingardi, A. Dummel, D. Falchero, M. Pidd, S.G. Voutsinas, J. Yin, "Aerodynamic Interference in Full Helicopter Configurations: Validation using the HeliNOVI Database", 32nd ERF, Maastricht, 2006

[22] J. Yin, A. Dummel, D. Falchero, M. Pidd, J. Prospathopoulos,A.Visingardi, S.G.

Voutsinas, “Analysis of Tail Rotor noise reduction benefits using HELINOVI aeroacoustic main/tail rotor test and posttest prediction results”, 32nd ERF, Maastricht, 2006
[23] A. Filippone, “Validation of post-test aerodynamic calculations with DNW PIV Data”, HeliNOVI deliverable D1.4-1, March 2006
[24] M. Pidd, “Final Validation Report of the Acoustic Prediction Codes”, HeliNOVI deliverable D1.4-3, March 2006
[25] O. Dieterich, I. Cafarelli, B. van der Wall, A. Visingardi, R. Bakker, S. Voutsinas, V. Riziotis, “Validation of Vibration Excitation Sources”, HeliNOVI deliverable D2.4, March 2006
[26] O. Dieterich, H.J. Langer, R. Bakker, “Correlation with flight test results”, HeliNOVI deliverable D2.6-2, March 2006